INTERNATIONAL JOURNAL FOR NUMERICAL METHODS IN FLUIDS, VOL. 22, 961–978 (1996)

PLANAR LIQUID SHEETS AT LOW REYNOLDS NUMBERS

J. I. RAMOS

Departamento de Lenguajes y Ciencias de la Computación, ETS Ingenieros Industriales, Universidad de Málaga, Plaza El Ejido, s/n, E-29013, Málaga, Spain

SUMMARY

Asymptotic methods are employed to derive the leading-order equations which govern the fluid dynamics of time-dependent, incompressible, planar liquid sheets at low Reynolds numbers using as small parameter the slenderness ratio. Analytical and numerical solutions of relevance to both steady film casting processes and plane stagnation flows are obtained with the leading-order equations. It is shown that for steady film casting processes the model which accounts for both gravity and low-Reynolds-number effects predicts thicker and slower planar liquid sheets than those which neglect a surface curvature term or assume that Reynolds number is zero, because the neglect of the curvature term and the assumption of zero Reynolds number are not justified at high take-up velocities owing to the large velocity gradients that occur at the take-up point. It is also shown that for Reynolds number/Froude number ratios larger than one, models which neglect the surface curvature or assume a zero Reynolds number predict velocity profiles which are either concave or exhibit an inflection point, whereas the model which accounts for both curvature and low-Reynolds-number effects predicts convex velocity profiles. For plane stagnation flows it is shown that models which account for both low-Reynolds-number and curvature effects predict nearly identical results to those of models which assume zero Reynolds number. These two models also predict a faster thickening of the planar liquid sheet than models which account for low-Reynolds-number effects but neglect the surface curvature. This curvature term is very large near the stagnation point and cannot be neglected there. It is also shown that the thickening of the sheet occurs closer to the stagnation point as the Reynolds number/Froude number ratio is increased, i.e. as the magnitude of the gravitational acceleration is increased. In addition it is shown that large surface tension introduces a third-order spatial derivative in the axial momentum equation at leading order.

KEY WORDS: planar liquid sheets; perturbation methods; film casting; film coating; plane stagnation flows

1. INTRODUCTION

In 1961 Taylor, in an appendix to Reference 1, used his characteristic skill and physical insight to obtain a partial differential equation which approximates the steady behaviour of a thin, incompressible, symmetric, planar liquid sheet. Taylor did not account for surface tension and assumed that the axial velocity component and the pressure are independent of the transverse co-ordinate. Clarke[2] studied steady, two-dimensional, planar, viscous flows falling from a nozzle under gravity, did not account for the relaxation of the flow from the no-slip boundary conditions at the nozzle walls to the free surface flow conditions downstream from the nozzle, employed complex variables and inner and outer expansions for low-Reynolds-number flows. His inner expansion accounted for gravity, viscosity and inertia and was expected to be accurate downstream from, but not near to, the nozzle. His outer expansion was based on the expectation that sufficiently far downstream from the nozzle exit the planar sheet becomes very thin and its dynamics are controlled by gravity and viscosity. This outer region is the one for which the equation obtained by Taylor is valid. Clarke[3] obtained the solution corresponding to his outer expansion in terms of Airy functions and matched it to his inner one.

CCC 0271–2091/96/100961–18

Received 24 May 1995
Revised 25 August 1995

More recently Aidun[4] used heuristic arguments and tried to use perturbation methods to study the steady dynamics of thin liquid films accounting for gravity, viscosity and surface tension. Unfortunately, he worked with dimensional variables, used an unspecified perturbation parameter and obtained the equation derived by Taylor.[1] By assuming thin, planar liquid sheets and neglecting the surface curvature, Aidun[4] obtained the solution of his equations in terms of Bessel functions for the case of no surface tension and showed that the neglect of surface curvature predicts an average liquid velocity in good accord with that of Taylor[1] for non-dimensional distances larger than about 10. It must be noted that Airy functions may be written in terms of Bessel ones[5] and that Aidun[4] dimensionalized the liquid velocity and co-ordinates in terms of the gravitational acceleration and the liquid kinematic viscosity; the same non-dimensionalization was employed by Taylor[1] and Clarke.[2] Cruickshank[6] used Taylor's equation and a low-Reynolds-number approximation in his studies of plane stagnation flows at low Reynolds numbers and obtained analytical solutions for a variety of boundary conditions.

In this paper, thin, planar liquid sheets consisting of an incompressible, constant density, viscous, isothermal, unsteady liquid exiting from a nozzle are analysed by means of perturbation methods based on the thickness of the sheet and a long-wave approximation as functions of the Reynolds, Froude and capillary numbers. The stick–slip problem and the relaxation of the flow as the fluid exits the nozzle are not considered and the gases surrounding the liquid are assumed to be dynamically passive. It is shown that the slender or long-wave approximation reduces the time-dependent, two-dimensional Navier–Stokes equations to a system of time-dependent, one-dimensional ones at leading order which have analytical solutions in some cases. These one-dimensional equations are employed to study steady, plane stagnation flows and steady film casting processes at low Reynolds numbers. Furthermore, using dimensionless variables based on the liquid axial velocity at the nozzle exit, the nozzle exit width and a long-wave approximation, the steady state equations obtained by Taylor[1] and Clarke[2] are derived and analytical solutions are obtained for planar sheets at zero Reynolds number without surface tension and for viscous–gravity sheets with and without surface tension.

The time-dependent formulation presented in this paper may be used to study film casting processes and their stability. The equations governing film casting were derived by Yeow,[7] who used essentially the same type of physical arguments as those employed by Taylor[1] and Matovich and Pearson;[8] the latter analysed fibre spinning processes of axisymmetric, viscous liquid jets.

Film casting processes consist essentially of a tank provided with a slot die through which a polymer melt is extruded. The melt may be guided by two wires, which are placed sufficiently far apart from each other, or unguided. The polymer film thus formed is cooled at a sufficiently fast rate so that it solidifies before reaching a rotating drum where it is collected (Figure 1). The film casting process is analogous to the fibre spinning processes used to obtain, for example, fibre glass and synthetic fibres such as nylon. Film casting processes are used to obtain aluminium foil and plastic films which are employed as wrapping materials. Note that an unguided, planar liquid sheet contracts in the longitudinal direction owing to surface tension (Figure 1).

Thin, viscous, planar liquid sheets or curtains have also been proposed and used as a way of applying protective organic coatings to continuous steel at high speed[1] and to deposit a thin, uniform film on a moving, solid substrate; their disintegration at high speeds is used to produce sprays for combustion, chemical engineering and agricultural applications, whereas their instabilities at low speeds result in the formation of ligaments due to capillary effects. These ligaments then break up and form droplets. The stability of planar liquid sheets is not considered in this paper.

In addition to the rigorous asymptotic derivation of the one-dimensional equations governing the dynamics of thin, planar liquid sheets, the approximations used by Aidun[4] and Cruickshank[6] are also considered and their accuracy is assessed in both film casting processes and plane stagnation flows at low Reynolds numbers.

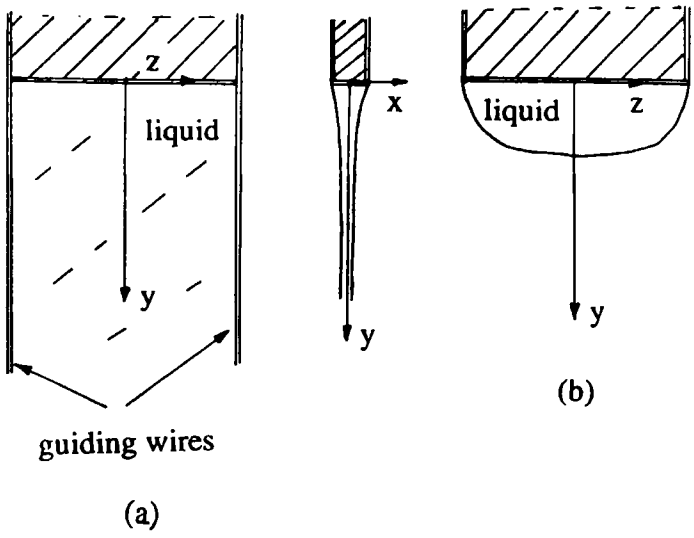

Figure 1. Schematics of a planar liquid sheet (a) guided by two wires and (b) unguided

The paper has been organized as follows. In the next section the dimensional Navier–Stokes equations in Cartesian co-ordinates and the boundary conditions for planar liquid sheets are presented. Asymptotic methods are employed in Section 3 to derive the leading-order equations which govern the fluid dynamics of planar liquid sheets by means of perturbation methods. In this section, Taylor's equation[1] is derived together with those for liquid sheets in zero gravity, sheets at low Reynolds numbers and viscous–gravity–capillary sheets. Applications of the one-dimensional equations derived in this paper to steady film casting processes and steady, plane stagnation flows are considered in Sections 4 and 5 respectively, together with some sample results. The last section of the paper summarizes the major conclusions.

2. FORMULATION

Consider an infinitely long planar liquid sheet or the planar liquid sheet guided by two wires shown schematically in Figure 1, where the wires are placed sufficiently far apart so that the flow may be considered two-dimensional, and assume that the fluid is incompressible (constant density), isothermal, two-dimensional and Newtonian, so that the conservation equations of mass and linear momentum can be written as

$$\frac{\partial u^*}{\partial x^*} + \frac{\partial v^*}{\partial y^*} = 0, \tag{1}$$

$$\rho^*\left(\frac{\partial u^*}{\partial t^*} + u^*\frac{\partial u^*}{\partial x^*} + v^*\frac{\partial u^*}{\partial y^*}\right) = -\frac{\partial p^*}{\partial x^*} + \mu^*\left(\frac{\partial^2 u^*}{\partial x^{*2}} + \frac{\partial^2 u^*}{\partial y^{*2}}\right) + \rho^* g^*, \tag{2}$$

$$\rho^*\left(\frac{\partial v^*}{\partial t^*} + u^*\frac{\partial v^*}{\partial x^*} + v^*\frac{\partial v^*}{\partial y^*}\right) = -\frac{\partial p^*}{\partial y^*} + \mu^*\left(\frac{\partial^2 v^*}{\partial x^{*2}} + \frac{\partial^2 v^*}{\partial y^{*2}}\right), \tag{3}$$

where t is time, u and v are the axial and transverse velocity components respectively, x and y are the axial and transverse co-ordinates respectively, ρ and μ are the fluid density and dynamic viscosity

respectively, p is the pressure, g is the gravitational acceleration and the asterisk denotes dimensional variables.

Equations (1)–(3) are subjected to symmetry conditions at the planar sheet axis, i.e.

$$\frac{\partial u^*}{\partial y^*}(x^*, 0, t^*) = \frac{\partial p^*}{\partial y^*}(x^*, 0, t^*) = v^*(x^*, 0, t^*) = 0, \tag{4}$$

and kinematic and dynamic boundary conditions at the sheet interface $y^* = h^*(x^*, t^*)$, where h^* denotes the local half-width of the planar liquid sheet. The kinematic condition establishes that the liquid–surroundings interface is a material surface where the shear stress is continuous and the jump in normal stresses across the interface must be balanced by surface tension. The kinematic and dynamic boundary conditions at the planar liquid sheet interface, i.e. at $y^* = h^*(x^*, t^*)$, are

$$v^* = \frac{\partial h^*}{\partial t^*} + u^* \frac{\partial h^*}{\partial x^*}, \tag{5}$$

$$2\mu^* \left(\frac{\partial v^*}{\partial y^*} - \frac{\partial u^*}{\partial x^*} \right) \frac{\partial h^*}{\partial x^*} + \mu^* \left(\frac{\partial u^*}{\partial y^*} + \frac{\partial v^*}{\partial x^*} \right) \left[1 - \left(\frac{\partial h^*}{\partial x^*} \right)^2 \right] = 0, \tag{6}$$

$$2\mu^* \frac{\partial u^*}{\partial x^*} \left(\frac{\partial h^*}{\partial x^*} \right)^2 - p^* \left[1 + \left(\frac{\partial h^*}{\partial x^*} \right)^2 \right] + 2\mu^* \frac{\partial v^*}{\partial y^*} - 2\mu^* \left(\frac{\partial u^*}{\partial y^*} + \frac{\partial v^*}{\partial x^*} \right) \frac{\partial h^*}{\partial x^*}$$

$$= -p_e^* \left[1 + \left(\frac{\partial h^*}{\partial x^*} \right)^2 \right] + \sigma^* \frac{\partial^2 h^* / \partial x^{*2}}{[1 + (\partial h^* / \partial x^*)^2]^{1/2}}, \tag{7}$$

where σ^* denotes the liquid surface tension and p_e^* is the pressure of the surroundings, which have been assumed to be dynamically passive. This assumption is justified, since if the surroundings are gases, they have, in general, smaller density and dynamic viscosity than those of liquids. This implies that the surrounding gases may not introduce strong velocity variations along each cross-section of the liquid sheet, although they may affect its dynamics.

In addition to the above symmetry, kinematic and dynamic boundary conditions, upstream conditions are required at the nozzle exit, whose width is $2h_0^*$. The boundary conditions at the nozzle exit are rather complex, since the flow relaxes from channel, i.e. no-slip, conditions to the kinematic and dynamic boundary conditions given by equations (5)–(7). Furthermore, if the liquid sheet were to be taken up by, say, a drum, additional boundary conditions would be needed downstream, i.e. at the drum. In order to satisfy the upstream and downstream boundary conditions, boundary layers may have to be introduced there and matched with the solution presented in this paper. Unfortunately, the equations governing these boundary layers are essentially the full governing equations, for which solutions may only be obtained numerically. This is avoided in this paper by simply imposing specified boundary conditions at the nozzle exit and downstream, as indicated later.

3. SLENDER LIQUID SHEETS

A liquid sheet is said to be slender when $\varepsilon = h_0^*/L^* \ll 1$, where L^* is a characteristic axial wavelength. For example, in film casting processes, L^* is the distance between the nozzle exit and the take-up drum. The above condition on ε also corresponds to a long-wave analysis of the governing equations.

We now introduce the non-dimensional variables

$$h = h^*/h_0^*, \qquad x = x^*/L^*, \qquad y = y^*/h_0^*,$$
$$u = u^*/u_0^*, \qquad p = p^*L^*/\mu^*\mu_0^*, \qquad t = t^*u_0^*/L^*, \tag{8}$$

so that the continuity equation may be written as

$$\frac{\partial u}{\partial x} + \frac{\partial v}{\partial y} = 0, \tag{9}$$

where

$$v^* = \varepsilon u_0^* v \tag{10}$$

and u_0^* denotes a (constant) reference axial velocity component.

The non-dimensional linear momentum equations may be written as

$$\varepsilon Re\left(\frac{\partial u}{\partial t} + u\frac{\partial u}{\partial x} + v\frac{\partial u}{\partial y}\right) = -\varepsilon^2\frac{\partial p^*}{\partial x^*} + \varepsilon^2\frac{\partial^2 u}{\partial x^2} + \frac{\partial^2 u}{\partial y^2} + \frac{Re}{Fr}, \tag{11}$$

$$\varepsilon Re\left(\frac{\partial v}{\partial t} + u\frac{\partial v}{\partial x} + v\frac{\partial v}{\partial y}\right) = -\frac{\partial p}{\partial y} + \varepsilon^2\frac{\partial^2 v}{\partial x^2} + \frac{\partial^2 v}{\partial y^2}, \tag{12}$$

while the non-dimensional kinematic and boundary conditions read as

$$v(x, h, t) = \frac{\partial h}{\partial t} + u(x, h, t)\frac{\partial h}{\partial x}, \tag{13}$$

$$2\varepsilon^2\left(\frac{\partial v}{\partial y} - \frac{\partial u}{\partial x}\right)\frac{\partial h}{\partial x} + \left(\frac{\partial u}{\partial y} + \varepsilon^2\frac{\partial v}{\partial x}\right)\left[1 - \varepsilon^2\left(\frac{\partial h}{\partial x}\right)^2\right] = 0, \tag{14}$$

$$2\varepsilon^2\frac{\partial u}{\partial x}\left(\frac{\partial h}{\partial x}\right)^2 + (p_e - p)\left[1 + \varepsilon^2\left(\frac{\partial h}{\partial x}\right)^2\right] + 2\frac{\partial v}{\partial y} - 2\left(\frac{\partial u}{\partial y} + \varepsilon^2\frac{\partial v}{\partial x}\right)\frac{\partial h}{\partial x} = \frac{\varepsilon}{Ca}\frac{\partial^2 h/\partial x^2}{[1 + \varepsilon^2(\partial h/\partial x^2]^{1/2}}, \tag{15}$$

where

$$Fr = \frac{u_0^{*2}}{g^* h_0^*}, \qquad Re = \frac{\rho^* u_0^* h_0^*}{\mu^*}, \qquad Ca = \frac{\mu^* u_0^*}{\sigma^*} \tag{16}$$

are the Froude, Reynolds and capillary numbers respectively.

For large Froude and small Reynolds numbers we assume that

$$Fr = F/\varepsilon, \qquad Re = \varepsilon R, \tag{17}$$

where F and R are of the order of one, so that the linear momentum equations, i.e. equations (11) and (12), become

$$\varepsilon^2 R\left(\frac{\partial u}{\partial t} + u\frac{\partial u}{\partial x} + v\frac{\partial u}{\partial y}\right) = -\varepsilon^2\frac{\partial p}{\partial x} + \varepsilon^2\frac{\partial^2 u}{\partial x^2} + \frac{\partial^2 u}{\partial y^2} + \varepsilon^2\frac{R}{F}, \tag{18}$$

$$\varepsilon^2 R\left(\frac{\partial v}{\partial t} + u\frac{\partial v}{\partial x} + v\frac{\partial v}{\partial y}\right) = -\frac{\partial p}{\partial y} + \varepsilon^2\frac{\partial^2 v}{\partial x^2} + \frac{\partial^2 v}{\partial y^2}. \tag{19}$$

3.1. Viscous–gravity liquid sheets

If there is no surface tension $Ca = \infty$ and the liquid sheet velocity components, pressure and half-width may be expressed as

$$u = u_0 + \varepsilon^2 u_2 + O(\varepsilon^2), \tag{20}$$

$$v = v_0 + \varepsilon^2 v_2 + O(\varepsilon^4), \tag{21}$$

$$p = p_0 + \varepsilon^2 p_2 + O(\varepsilon^4), \tag{22}$$

$$h = h_0 + \varepsilon^2 h_2 + O(\varepsilon^4). \tag{23}$$

Substitution of equations (20)–(23) into the continuity (equation (9)) and linear momentum (equations (18) and (19)) equations yields the following sequence of problems.

To $O(\varepsilon^0)$:

$$\frac{\partial u_0}{\partial x} + \frac{\partial v_0}{\partial y} = 0, \tag{24}$$

$$\frac{\partial^2 u_0}{\partial y^2} = 0, \tag{25}$$

$$-\frac{\partial p_0}{\partial y} + \frac{\partial^2 v_0}{\partial y^2} = 0. \tag{26}$$

To $O(\varepsilon^2)$:

$$\frac{\partial u_2}{\partial x} + \frac{\partial v_2}{\partial y} = 0, \tag{27}$$

$$R\left(\frac{\partial u_0}{\partial t} + u_0 \frac{\partial u_0}{\partial x} + v_0 \frac{\partial u_0}{\partial y}\right) = -\frac{\partial p_0}{\partial x} + \frac{\partial^2 u_0}{\partial x^2} + \frac{R}{F} + \frac{\partial^2 u_2}{\partial y^2}, \tag{28}$$

$$R\left(\frac{\partial v_0}{\partial t} + u_0 \frac{\partial v_0}{\partial x} + v_0 \frac{\partial v_0}{\partial y}\right) = -\frac{\partial p_2}{\partial y} + \frac{\partial^2 v_0}{\partial x^2} + \frac{\partial^2 v_2}{\partial y^2}. \tag{29}$$

Substitution of equations (20)–(23) into the kinematic and dynamic boundary conditions, i.e. equations (13)–(15), and expansion of the variables at (x, h, t) in Taylor series around (x, h_0, t) yield the following sequence problems.

To $O(\varepsilon^0)$:

$$v_0(x, h_0, t) = \frac{\partial h_0}{\partial t} + u_0(x, h_0, t)\frac{\partial h_0}{\partial x}, \tag{30}$$

$$\frac{\partial u_0(x, h_0, t)}{\partial y} = 0, \tag{31}$$

$$(p_e - p_0) + 2\frac{\partial v_0}{\partial y} - 2\frac{\partial h_0}{\partial x}\frac{\partial u_0}{\partial y} = 0, \tag{32}$$

To $O(\varepsilon^2)$:

$$v_2(x, h_0, t) + h_2 \frac{\partial v_0(x, h_0, t)}{\partial y} = \frac{\partial h_2}{\partial t} + \left(u_2(x, h_0, t) + h_2 \frac{\partial u_0(x, h_0, t)}{\partial y}\right) \frac{\partial h_0}{\partial x} + u_0(x, h_0, t) \frac{\partial h_2}{\partial x}, \tag{33}$$

$$2\left(\frac{\partial v_0}{\partial y} - \frac{\partial u_0}{\partial y}\right) \frac{\partial h_0}{\partial x} - \frac{\partial u_0}{\partial y} \left(\frac{\partial h_0}{\partial x}\right)^2 + \frac{\partial u_2}{\partial y} + \frac{\partial v_0}{\partial x} + h_2 \frac{\partial^2 u_0}{\partial y^2} = 0. \tag{34}$$

The boundary conditions at the symmetry axis can be expressed as

$$v_i = \frac{\partial u_i}{\partial y} = \frac{\partial p_i}{\partial y} = 0, \quad i = 0, 1, 2, \ldots, \quad \text{at} \quad y = 0. \tag{35}$$

The solution of equation (25) subject to equation (31) is

$$u_0 = B(x, t), \tag{36}$$

i.e. to leading order the axial velocity is independent of the transverse co-ordinate.

The solutions of equations (26) and (24) subject to equation (35) are respectively

$$p_0 = D(x, t), \qquad v_0 = -B'(x, t)y, \tag{37}$$

where the prime denotes partial differentiation with respect to x.

Equations (36) and (37) have been obtained here by means of perturbation methods and coincide with those derived by Taylor[1] and Yeow,[7] who developed one-dimensional equations to study thin liquid sheets by assuming that both the axial velocity component and the pressure are functions of the axial co-ordinate. As has been shown here, these assumptions are consistent with the leading-order expansions presented in this paper.

The solutions of equations (28) and (27) subject to equation (35) are respectively

$$u_2 = \frac{E(x, t)}{2} y^2 + G(x, t), \qquad v_2 = -\frac{E'(x, t)}{6} y^3 - G'(x, t)y, \tag{38}$$

where

$$E = R\left(\frac{\partial B}{\partial t} + B\frac{\partial B}{\partial x}\right) + \frac{\partial D}{\partial x} - \frac{R}{F} - \frac{\partial^2 B}{\partial x^2} \tag{39}$$

and $G(x, t)$ is a function which may be determined at higher order in the asymptotic expansion.

Substitution of equations (36) and (37) into equation (30) yields

$$\frac{\partial h_0}{\partial t} + \frac{\partial (B h_0)}{\partial x} = 0, \tag{40}$$

while equation (32) results in

$$p_e - p_0 + 2\frac{\partial v_0}{\partial y} - 2\frac{\partial h_0}{\partial x}\frac{\partial u_0}{\partial y} = 0, \tag{41}$$

which implies that

$$D = p_e - 2B'. \tag{42}$$

Finally equation (34) becomes

$$R\left(\frac{\partial (B h_0)}{\partial t} + \frac{\partial (B^2 h_0)}{\partial x}\right) = \frac{R}{F} h_0 + 4\frac{\partial [(\partial B/\partial x) h_0]}{\partial x}. \tag{43}$$

For steady, viscous–gravity, planar liquid sheets, equations (40) and (43) become

$$Bh_0 = C_1, \qquad R\frac{dB}{dx} - \frac{R}{F}\frac{1}{B} - 4\frac{d[(1/B)\,dB/dx]}{dx} = 0, \tag{44}$$

where C_1 is an integration constant.

Equation (44) coincides with that derived by Taylor by means of physical arguments. In fact, Taylor's equation,[1] i.e.

$$\frac{db}{dX} - \frac{1}{b} - \frac{d[(1/b)\,db/dX]}{dX} = 0, \tag{45}$$

can be obtained from equation (44) by transforming the dependent and independent variables as

$$B = b\left(\frac{4}{RF}\right)^{1/3}, \qquad x = X\left(\frac{16F}{R^2}\right)^{1/3}. \tag{46}$$

Clarke[2] also derived equation (45) by means of perturbation methods using a low-Reynolds-number approximation and the dimensionless variables defined in equation (46). Clarke[3] obtained the solution to equation (45) in terms of Airy functions. The solution of equation (44) may be written as

$$B = b\left(\frac{4}{RF}\right)^{1/3}, \qquad x = X\left(\frac{F}{R^2}\right)^{1/3}, \tag{47}$$

where

$$b = \frac{1}{f}, \qquad f = 2^{1/3}\frac{[C_1 Ai'(r) + C_2 Bi'(r)]^2}{[C_1 Ai(r) + C_2 Bi(r)]^2} - t, \tag{48}$$

$$r = 2^{-1/3}t, \qquad t = X + C, \tag{49}$$

C, C_1 and C_2 are integration constants that are to be determined from the upstream and downstream boundary conditions and Ai and Bi are Airy functions.[5]

In order that the time-dependent, one-dimensional equations derived in this section be valid, it is required that the $O(\varepsilon^2)$ and higher-order terms of the asymptotic expansion be small. In particular, if only two terms are kept in the asymptotic expansion, the one-dimensional equations are valid provided that the following conditions are met:

$$\varepsilon^2|\phi_2(x, y, t)| \ll |\phi_0(x, t)|, \tag{50}$$

where ϕ denotes u, v, p and h.

Equation (50) provides the values of ε for which the asymptotic expansion is valid. Furthermore, the perturbation method presented here permits us to calculate higher-order terms which will depend on the transverse co-ordinate as indicated in equation (38).

3.2. Viscous liquid sheets in zero gravity

In the absence of both surface tension and gravity, i.e. $Ca = \infty$ and $Fr = \infty$ respectively, equation (44) become

$$Bh_0 = C_1, \qquad RB - \frac{4}{B}\frac{dB}{dx} = C_2, \tag{51}$$

where C_2 is an integration constant.

The solution of equation (51) is

$$\frac{B}{B - C_2/R} = C_3 e^{-C_2 x/4}, \tag{52}$$

where C_3 is an integration constant.

3.3. *Liquid sheets at Re = 0*

When the Reynolds number is zero, i.e. when the inertia of the flow is zero, equation (44) become

$$Bh_0 = C_1, \qquad \frac{1}{B}\frac{dB}{dx} = C_4, \tag{53}$$

the solutions of which are

$$B = C_5 e^{C_4 x}, \qquad h_0 = \frac{C_1}{C_5} e^{-C_4 x}, \tag{54}$$

where C_4 and C_5 are integration constants.

The leading-order equations presented in the previous subsections are valid not only for $Ca = \infty$ but also for $Ca = C/\varepsilon$ provided that $C = O(1)$, showing that small values of the surface tension do not affect the leading-order terms in the perturbation expansion.

3.4. *Viscous–gravity–capillary planar liquid sheets*

If the capillary number $Ca = \varepsilon C$, where $C = O(1)$, substitution of equations (20)–(23) into the governing equations and the boundary conditions yields the same equations to $O(\varepsilon^0)$ as those derived above, except for the normal stress condition, i.e. equation (32), which becomes, to this order,

$$p_e - p_0 + 2\frac{\partial v_0}{\partial y} - 2\frac{\partial h_0}{\partial x}\frac{\partial u_0}{\partial y} = \frac{1}{C}\frac{\partial^2 h_0}{\partial x^2}. \tag{55}$$

Proceeding in an analogous manner to that used in the previous subsections, one obtains

$$R\left(\frac{\partial(Bh_0)}{\partial t} + \frac{\partial(B^2 h_0)}{\partial x}\right) = \frac{R}{F}h_0 + 4\frac{\partial[(\partial B/\partial x)h_0]}{\partial x} + \frac{1}{C}h_0\frac{\partial^3 h_0}{\partial x^3}, \tag{56}$$

$$\frac{\partial h_0}{\partial t} + \frac{\partial(Bh_0)}{\partial x} = 0. \tag{57}$$

Equation (56) indicates that the effects of surface tension introduce a third-order spatial derivative.

3.5. *Liquid sheets at Re = 0 with finite R/F*

If the Reynolds number is zero, but R/F is finite, equation (44) may be written as

$$4\frac{d}{dx}\left(\frac{1}{B}\frac{dB}{dx}\right) + \frac{R}{F}\frac{1}{B} = 0, \tag{58}$$

which may be reduced to the following first-order, ordinary differential equation by means of the transformations $dB/dx = Q$ and $Q = P^2$:

$$dx = \frac{dB}{[B^2 C + (R/2F)B]^{1/2}}, \tag{59}$$

where C is an integration constant.

If $C=0$, the solution of equation (59) may be written as

$$B=\left[1+\left(\frac{2R}{F}\right)^{1/2}x\right]^2, \tag{60}$$

where we have set $B(0)=1$. This solution cannot be used to study film casting processes or plane stagnation flows which are characterized by two-point boundary value problems, because it has no free constant with which the downstream boundary condition may be satisfied.

If $C\neq 0$, the solution of equation (59) subject to $B(0)=1$ may be expressed as[9]

$$B=\frac{qe^{qx}}{C+q-Ce^{qx}}, \tag{61}$$

where $q=R/2F$.

Equation (58) has also been considered by Cruickshank[6] in his studies of plane stagnation flows, although he used a different non-dimensionalization from the one employed here and did not recognize that this equation corresponds to zero Reynolds number and finite R/F.

3.6. *Free-falling liquid sheets*

The axial velocity component of free-falling liquid sheets can be derived from equation (44) by setting $R=\infty$ and $B(0)=1$. This results in

$$B=\left(1+\frac{2x}{F}\right)^{1/2}, \tag{62}$$

which is Torricelli's free-fall law and agrees with the solution of Taylor's equation for non-dimensional axial distances greater than about 10 if the non-dimensionalization is performed according to equation (46). In fact, Taylor's equation[1] has usually been solved subject to a downstream boundary condition which corresponds to either experimental data or the free-fall velocity.

3.7. *Aidun's approximation*

Equation (44) may be written as

$$\frac{d^2B}{dx^2}-\frac{1}{B}\left(\frac{dB}{dx}\right)^2+\frac{R}{4F}=\frac{RB}{4}\frac{dB}{dx}. \tag{63}$$

Aidun,[4] perhaps unaware of the solution obtained by Clarke,[3] neglected the second term on the left-hand side of the above equation and obtained an analytical solution using the dimensionless variables given by equation (46). Here we first integrate equation (63) to obtain

$$\frac{dB}{dx}+\frac{R}{4F}x=\frac{R}{8}B^2+C, \tag{64}$$

where C is an integration constant. We then transform the independent and dependent variables as

$$x=\frac{8z}{R}+\frac{4FC}{R}, \qquad B=-\frac{\psi'}{\psi}, \qquad z=\left(\frac{FR}{16}\right)^{1/3}y \tag{65}$$

to obtain

$$\frac{d^2\psi}{dy^2}-y\psi=0, \tag{66}$$

which is Airy's equation, whose solution may be written as[5]

$$\psi = C_1 Ai(y) + C_2 Bi(y), \tag{67}$$

where C_1 and C_2 are constants that must be determined from the upstream and downstream boundary conditions.

It must be noted that $Ai(y)$ and $Ai'(y)$ respectively decrease and increase monotonically to zero, whereas both $Bi(y)$ and $Bi'(y)$ increase monotonically with y.[5]

Aidun's approximation[4] can only be justified if the surface curvature term neglected in equation (63) is indeed much smaller than the terms retained in that equation. For free-falling liquid sheets this approximation may be an accurate one, since the neglected term is small and decreases as x increases. This may explain why the results of Aidun[4] agree with the experimental ones of Brown[1] for axial distances greater than about 8 when the non-dimensionalization is performed according to equation (46).

The models presented in this section, except for that of Section 3.6, may be used to analyse steady film casting processes, steady, plane stagnation flows and semi-infinite planar liquid sheets. The only differences between these flows occur in the downstream boundary conditions. Semi-infinite planar liquid sheets have been considered by Brown[1] and Aidun,[4] who used experimentally measured data and the free-fall velocity law (see equation (62)) respectively for the downstream boundary conditions. In the next sections, film casting processes and plane stagnation flows are considered.

4. APPLICATION TO STEADY FILM CASTING PROCESSES

In the previous section the upstream and downstream boundary conditions were in most cases left unspecified. Here we present the boundary conditions relevant to film casting processes. Since, in general, $u^*(0, y^*, t^*)$ is a function of y^* and t^* and boundary layers may be formed at both the nozzle exit and the take-up drum, rather than imposing values of $u^*(0, y^*, t^*)$ and $u^*(L^*, y^*, t^*)$, where L^* denotes the axial distance from the nozzle exit to the take-up drum, we will impose integral conditions of the form

$$2\int_0^{h_0^*} u^*(0, y^*, t^*)\,dy^* = q^*(t^*), \tag{68}$$

$$2\int_0^{h^*(L^*,t^*)} u^*(L^*, y^*, t^*)\,dy^* = Q^*(t^*), \tag{69}$$

which can be written in non-dimensional form as

$$2\int_0^1 u(0, y, t)\,dy = q, \tag{70}$$

$$2\int_0^{h(1)} u(1, y, t)\,dy = Q, \tag{71}$$

where $q = q^*/h_0^* u_0^* = q(t)$ and $Q = Q^*/h_0^* u_0^*$. Note that $q = Q$ for steady sheets.

Equation (69) may also be replaced by a take-up form at the drum.

Substitution of equation (20) into equations (70) and (71) yields to $O(\varepsilon^0)$, i.e. to leading order,

$$2\int_0^1 u_0(0,t)\,dy = q, \tag{72}$$

$$2\int_0^{h_0(1)} u_0(1,t)\,dy = Q, \tag{73}$$

where the last equation has been obtained from equation (71) by using Taylor series expansions. Note that equations (68), (70) and (72) assume that the liquid attaches to the nozzle sharp corner.

Using the results from the previous section, equations (72) and (73) yield

$$B(0,t) = q/2, \qquad B(1,t) = Q/2h_0(1). \tag{74}$$

For steady, viscous liquid sheets at zero Reynolds number (see Section 3.3), $q = Q = 2$ and

$$B(x) = e^{\delta x}, \tag{75}$$

where $B(1) = e^{\delta}$ is the drum speed. Note that $\delta = -\ln h(1)$; therefore

$$B(x) = \left(\frac{1}{h(1)}\right)^x, \qquad h(x) = [h(1)]^x. \tag{76}$$

For steady state, viscous liquid sheets in zero gravity with zero surface tension (see Section 3.2), $q = Q = 2$ and the axial velocity of the liquid is given by equation (52) with

$$C_3 = \frac{R}{C_2 - R}, \qquad C_2 = -4\left[\ln B(1) + \ln\left(\frac{RB(1) - C_2}{R - C_2}\right)\right]. \tag{77}$$

It may also be shown that the value of C in equation (61) is given by

$$C = \frac{q[e^q - B(1)]}{B(1)(1 - e^q)}, \tag{78}$$

while the values of C_1 and C_2 in equations (48) and (67) may be easily determined from the conditions $B(0) = 1$ and $B(1)$.

Equation (44) was solved numerically by means of a second-order, central finite difference method. The same numerical method was used to determine the solutions of the equations presented in Sections 3.2, 3.5 and 3.7 and the results obtained have been compared with those for equation (44). The step size was varied so as to avoid non-linear oscillations and obtain accurate results. Most of the computations presented here were performed with $\Delta x = 0{\cdot}001$.

Some sample results are presented in Figures 2–7. Figures 2 and 3 show the leading-order axial velocity component and sheet thickness as a function of the vertical co-ordinate for $h_0(1) = 0{\cdot}1$ and $0{\cdot}01$ respectively. These figures illustrate the steepening of both the axial velocity and sheet thickness at the take-up point as the drum velocity is increased. They also show that the velocity of zero-Reynolds-number sheets (see Section 3.3) is larger than that of viscous sheets with $R = 1$ in zero gravity (see Section 3.2). The latter exhibit steeper gradients than the former at the downstream boundary. Figures 2 and 3 also show the free-fall velocity predictions for comparison.

Figures 4–7 illustrate the effects of R/F and $h_0(1)$ on the predictions of the models presented in Sections 3.5, 3.1 and 3.7. For the models of Sections 3.1 and 3.7, R was set to unity. Figure 4 indicates that for $h_0(1) = 0{\cdot}1$ and $R/F = 1$ the model of Section 3.7 predicts higher axial velocities than those of Sections 3.5 and 3.1. However, for $h_0(1) = 0{\cdot}01$ and $R/F = 1$ (see Figure 5) the model of Section 3.7 predicts respectively higher and lower axial velocities than those of Section 3.5 for $x \leqslant 0{\cdot}5$ and $x \geqslant 0{\cdot}5$ respectively. The velocity predictions of the model of Section 3.1 lie below those of the other models.

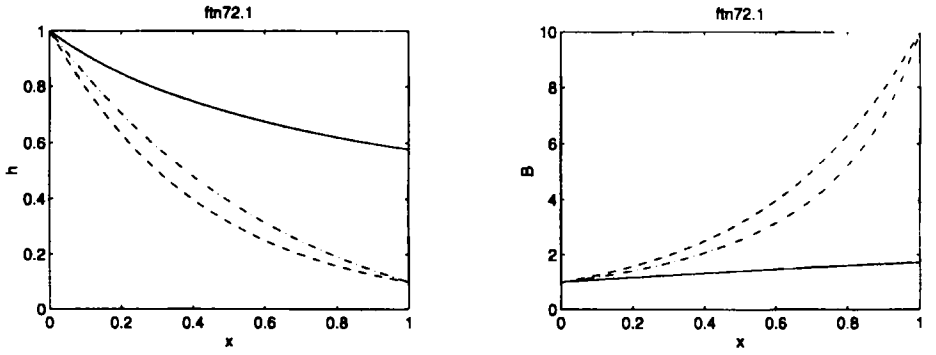

Figure 2. Leading-order thickness (left) and axial velocity component (right) as functions of vertical co-ordinate x in film casting processes (————, model of Section 3.6; – – – –, model of Section 3.3; – · – · –, model of Section 3.2; $h_0(1) = 0{\cdot}1$)

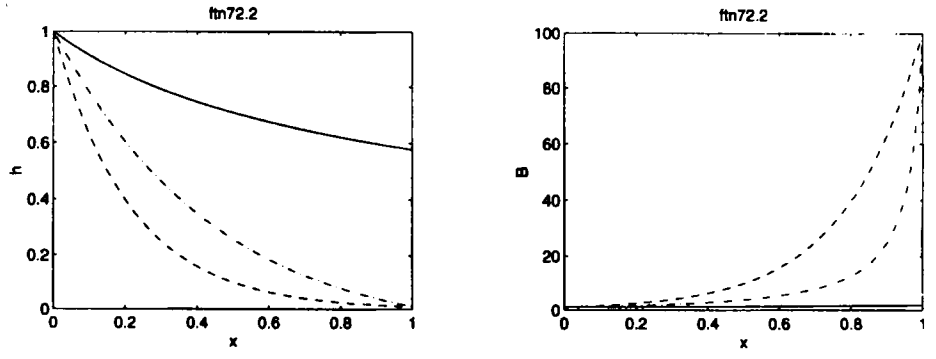

Figure 3. Leading-order thickness (left) and axial velocity component (right) as functions of vertical co-ordinate x in film casting processes (————, model of Section 3.6; – – – –, model of Section 3.3; – · – · –, model of Section 3.2; $h_0(1) = 0{\cdot}01$)

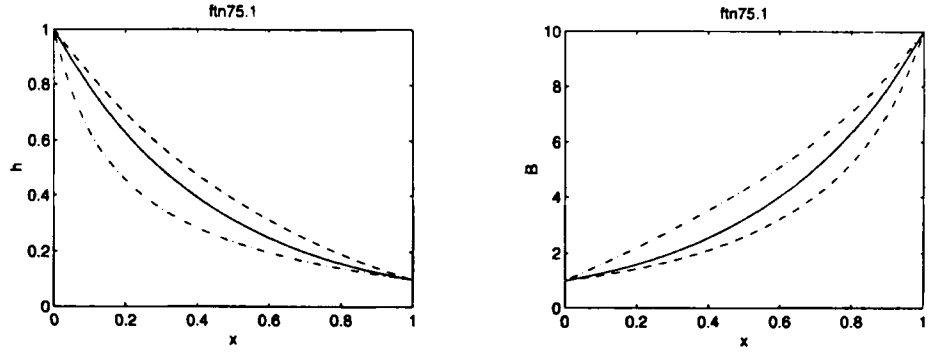

Figure 4. Leading-order thickness (left) and axial velocity component (right) as functions of vertical co-ordinate x in film casting processes (——, model of Section 3.7; – – –, model of Section 3.1 with $R = 1$; – · – · –, model of Section 3.5 with $R = 0$; $h_0(1) = 0{\cdot}1$; $R/F = 100$)

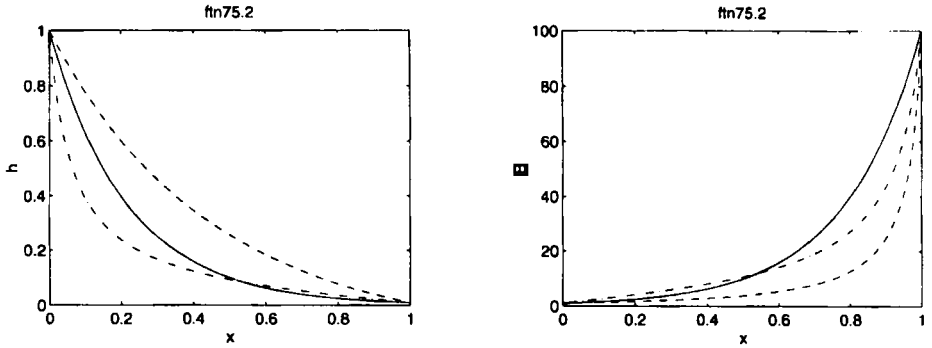

Figure 5. Leading-order thickness (left) and axial velocity component (right) as functions of vertical co-ordinate x in film casting processes (————, model of Section 3.7; – – – –, model of Section 3.1 with $R=1$; – · – · –, model of Section 3.5 with $R=0$; $h_0(1)=0{\cdot}01$; $R/F=1$)

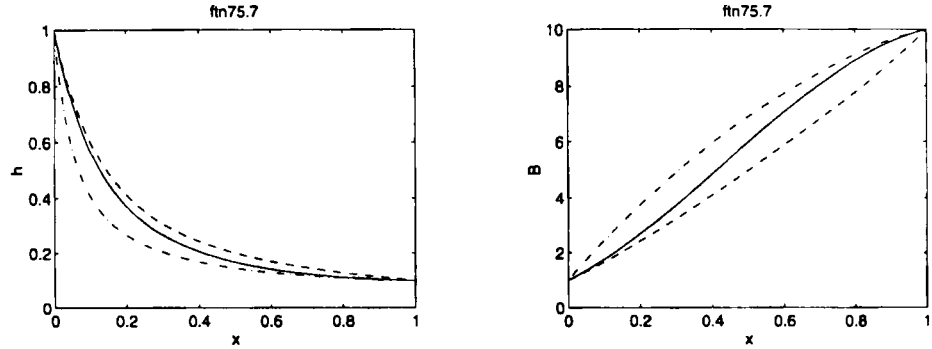

Figure 6. Leading-order thickness (left) and axial velocity component (right) as functions of vertical co-ordinate x in film casting processes (————, model of Section 3.7; – – – –, model of Section 3.1 with $R=1$; – · – · –, model of Section 3.5 with $R=0$; $h_0(1)=0{\cdot}1$; $R/F=100$)

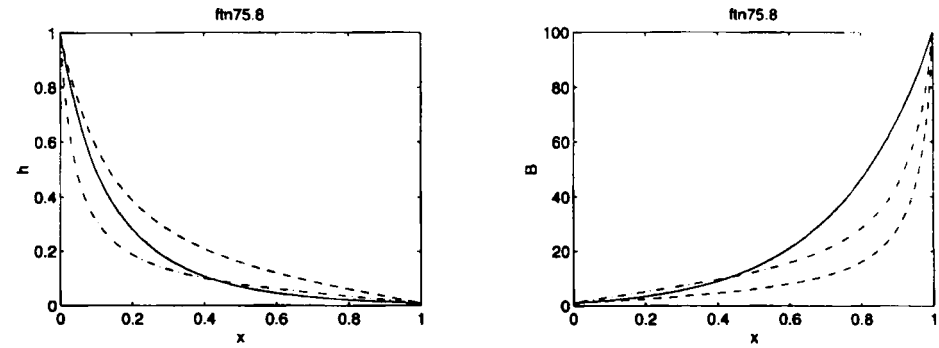

Figure 7. Leading-order thickness (left) and axial velocity component (right) as functions of vertical co-ordinate x in film casting processes (————, model of Section 3.7; – – – –, model of Section 3.1 with $R=1$; – · – · –, model of Section 3.5 with $R=0$; $h_0(1)=0{\cdot}01$; $R/F=100$)

Similar results have been obtained for $R/F < 1$. In fact, the results for $R/F = 0{\cdot}01$ are indistinguishable from those presented in Figures 4 and 5.

Figures 6 and 7 correspond to $R/F = 100$ and $h_0(1) = 0{\cdot}1$ and $0{\cdot}01$ respectively. Figures 5 and 7 indicate that the agreement between the models of Sections 3.5 and 3.7 improves as R/F is increased for high take-up velocities. However, for lower take-up velocities (see Figures 4 and 6) the results presented in Figure 6 indicate that the concavity of the axial velocity curves predicted by the models of Sections 3.5 and 3.7 is different from those presented in Figures 4, 5 and 7. In fact, the axial velocity component predicted by the model of Section 3.5 exhibits an inflection point at about $x = 0{\cdot}5$, whereas that of the model of Section 3.7 is concave downwards.

5. STEADY PLANE STAGNATION FLOWS

In plane stagnation flows, $B(1) = 0$ and $h_0(1) = \infty$, while the boundary conditions at the nozzle exit are $B(0) = h_0(0) = 1$. For these flows one can obtain analytical solutions to the equations presented in Section 3. Equation (44) and those of Sections 3.2, 3.5 and 3.7 were solved numerically using a second-order-accurate, central finite difference method subject to $B(0) = 1$ and $B(1) = 0$ for different values of R/F.

Figures 8–10 show the leading-order thickness and axial velocity component calculated with the models presented in Sections 3.7, 3.5 and 3.1 as functions of x for $R/F = 1$, $0{\cdot}01$ and 100 respectively. These figures indicate that the model of Section 3.7 underpredicts the sheet thickness, whereas those of Sections 3.1 and 3.5 yield nearly identical results. These figures also indicate that the axial velocity predicted by the model of Section 3.7 is nearly a linear function of x and that the models of Sections 3.5 and 3.7 predict a fast thickening of the planar sheet near the nozzle exit for $R/F \leqslant 1$ (see Figures 8 and 9). For $R/F = 100$ the results presented in Figure 10 indicate that the sheet thickness first decreases and then increases as a function of x. This figure also indicates that the differences between the predictions of the models of Sections 3.1 and 3.5 are very small, while the predictions of the model presented in Section 3.7 indicate a smaller rate of thickening. It must be pointed out that the model of Section 3.7 neglected a surface curvature term which is not at all negligible for x approximately equal to zero. Therefore the validity of this model is rather questionable in that region.

Figure 11 shows the results of the model presented in Section 3.2 for $R = 1$. This model predicts a larger thickening of the planar liquid sheet close to the nozzle exit than those observed in Figures 8–10 and this result is not surprising in view of the fact that the model of Section 3.7 does not account for the

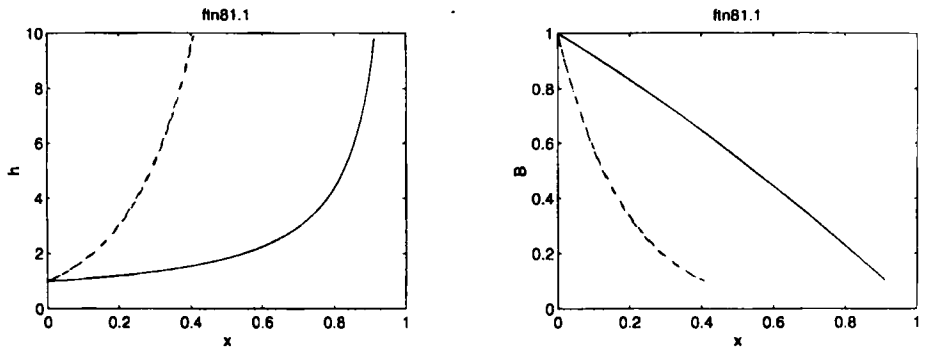

Figure 8. Leading-order thickness (left) and axial velocity component (right) as functions of vertical co-ordinate x for plane stagnation flows (————, model of Section 3.7; – – – –, model of Section 3.1 with $R = 1$; – · – · –, model of Section 3.5 with $R = 0$; $R/F = 1$)

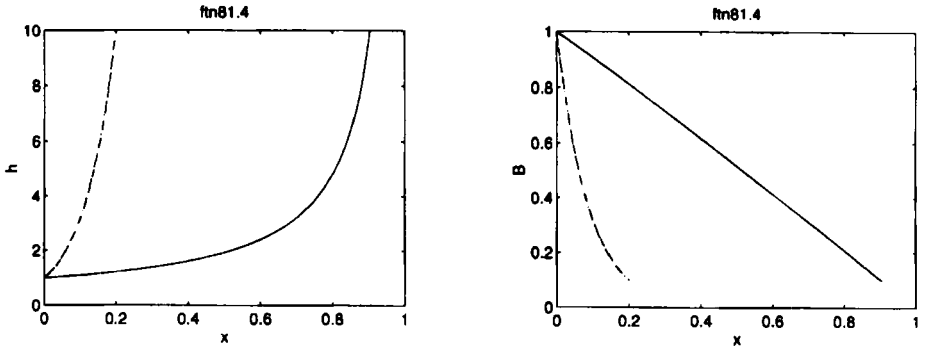

Figure 9. Leading-order thickness (left) and axial velocity component (right) as functions of vertical co-ordinate x for plane stagnation flows (————, model of Section 3.7; – – – –, model of Section 3.1 with $R=1$; – · – · –, model of Section 3.5 with $R=0$; $R/F=0{\cdot}01$)

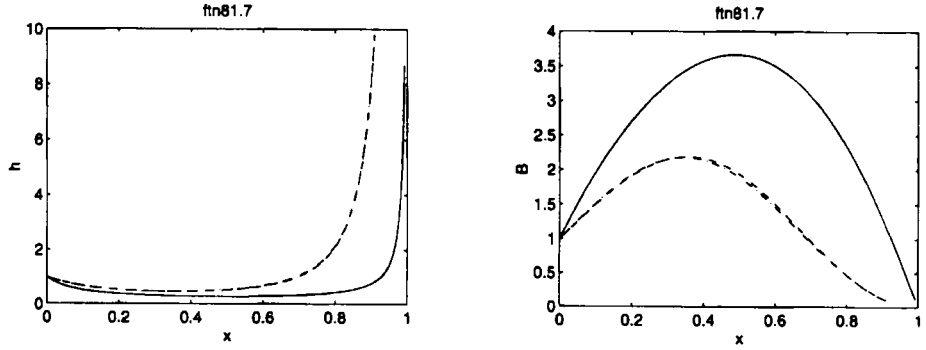

Figure 10. Leading-order thickness (left) and axial velocity component (right) as functions of vertical co-ordinate x for plane stagnation flows (————, model of Section 3.7; – – – –, model of Section 3.1 with $R=1$; – · – · –, model of Section 3.5 with $R=0$; $R/F=100$)

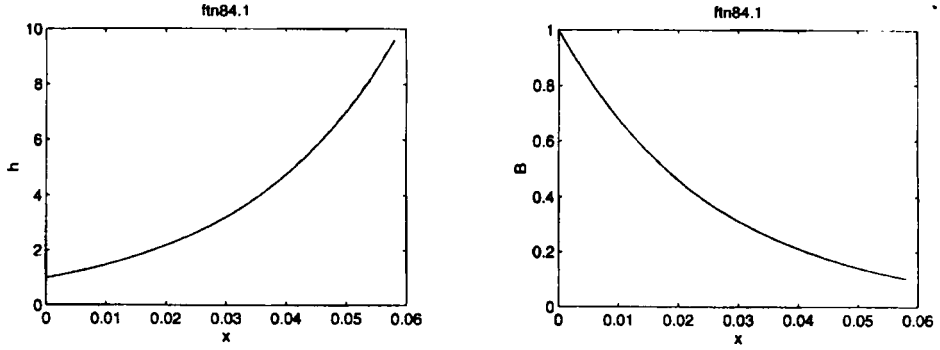

Figure 11. Leading-order thickness (left) and axial velocity component (right) as functions of vertical co-ordinate x for plane stagnation flows predicted by the model of Section 3.2 with $R=1$)

gravitational pull. It must be noted that the model of Section 3.3 is not applicable to plane stagnation flows because it cannot satisfy the upstream and downstream boundary conditions.

It must be pointed out that the validity of the slender flow approximation employed in this paper may not be justified in plane stagnation flows owing to the large increase in the sheet thickness. Furthermore, these flows are two-dimensional and may require a two-dimensional analysis, especially near the stagnation point where the transverse velocity component is of the same order of magnitude as or larger than the axial one, whereas the models derived in this paper are one-dimensional and are strictly valid for slender flows, i.e. flows were the transverse velocity is much smaller than the axial one.

6. CONCLUSIONS

Perturbation methods based on the slenderness ratio have been employed to determine the leading-order equations governing the fluid dynamics of incompressible, isothermal, planar liquid sheets at low Reynolds numbers as a function of the Froude and capillary numbers. Analytical solutions for viscous sheets in gravitational and zero-gravity environments have been obtained. Analytical and numerical solutions of both steady film casting processes and steady plane stagnation flows have also been obtained. In film casting processes it has been shown that the model which accounts for both gravity and low-Reynolds-number effects predicts thicker and slower planar liquid sheets than those which neglect a surface curvature term or assume that the Reynolds number is zero, because the neglect of the curvature term and the assumption of zero Reynolds number are not justified at high take-up velocities owing to the large velocity gradients that occur at the take-up point. It has also been shown that for Reynolds number/Froude number ratios larger than one, models which neglect the surface curvature or assume a zero Reynolds number predict velocity profiles which are either concave or exhibit an inflection point respectively, whereas the model which accounts for both curvature and low-Reynolds-number effects predicts convex velocity profiles.

Although analytical solutions to the leading-order axial velocity component and sheet thickness may be readily obtained in some cases in terms of Airy functions, the use of a second-order-accurate finite difference for plane stagnation flows indicates that models which account for both low-Reynolds-number and curvature effects predict nearly identical results to those of models which assume zero Reynolds number. These two models also predict a faster thickening of the planar liquid sheet than models which account for low-Reynolds-number effects but neglect the surface curvature. This curvature term is very large near the stagnation point and cannot be neglected there. It has also been shown that the thickening of the sheet occurs closer to the stagnation point as the Reynolds number/Froude number ratio is increased, i.e. as the magnitude of the gravitational acceleration is increased.

Finally, it has been shown that large surface tension introduces a third-order spatial derivative in the axial momentum equation at leading order.

ACKNOWLEDGEMENT

The research reported in this paper was supported by Project PB91-0767 from the DGICYT of Spain.

REFERENCES

1. D. R. Brown, 'A study of the behaviour of a thin sheet of moving liquid', *J. Fluid Mech.*, **10**, 297–305 (1961).
2. N. S. Clarke, 'Two-dimensional flow under gravity in a jet of viscous liquid', *J. Fluid Mech.*, **31**, 481–500 (1968).
3. N. S. Clarke, 'A differential equation in fluid mechanics', *Mathematika*, **12**, 51–53 (1966).

4. C. K. Aidun, 'Mechanics of a free-surface liquid film flow', *ASME J. Appl. Mech.*, **54**, 951–954 (1987).
5. M. Abramowitz and I. A. Stegun, *Handbook of Mathematical Functions*, Dover, New York, 1972.
6. J. O. Cruickshank, 'A similarity between plane and axisymmetric viscous–gravity jets', *Trans. ASME, J. Fluids Eng.*, **106**, 52–53 (1984).
7. Y. L. Yeow, 'On the stability of extending films: a model for the film casting process', *J. Fluid Mech.*, **66**, 613–622 (1974).
8. M. A. Matovich and J. R. Pearson, 'Spinning a molten threadline', *Ind. Eng. Chem. Fund.*, **8**, 512–520 (1969).
9. H. B. Dwight, *Tables of Integrals and Other Mathematical Data*, 4th edn, MacMillan, New York, 1961.